Molecular Dynamics Simulations of Surface Chemical Reactions

Barbara J. Garrison
Department of Chemistry, The Pennsylvania State University, University Park, PA 16802, U.S.A.

1 Introduction

Within the framework of classical mechanics, molecular dynamics simulations yield an essentially exact method for observing the dynamics of atoms and molecules during complex chemical reactions. Consequently, this technique can be used to study a wide range of dynamical events which are associated with surfaces. For example, the atomic motions which lead to the ejection of surface species during keV particle bombardment (sputtering) have been identified using molecular dynamics (MD) simulations, and these results have been directly correlated with various experimental observations.[1] Often such simulations provide the only direct link between experimentally measured macroscopic quantities and microscopic chemical dynamics.

In its pure classical form, molecular dynamics is straightforward to carry out. For a system of interest, one starts with a given set of initial conditions, which include the atomic positions, velocities, and forces which are derived from interaction potentials. For example, to simulate a sputtering event, the initial conditions might correspond to a collection of atomic coordinates which comprise the solid surface and the incoming energetic particle (Figure 1). The dynamics are then determined by numerically solving a set of classical equations of motion. Various aspects of the dynamics, such as reaction mechanisms and product distributions, can then be determined by examining the motions of the atoms during the simulation. In this process, all that is assumed is the validity of classical mechanics and the quality of the interaction potential being used. The former approximation, although never totally true, is reasonably well understood. An indicator of the validity of classical mechanics is the deBroglie wavelength, $\lambda = \hbar/\sqrt{(2mE)}$, of the moving particle. Here $\hbar$ is Planck's constant, m is the mass of the particle, and E is its kinetic energy. For a particle moving with a kinetic energy of 1 eV, the deBroglie wavelength of the particle is 12 Å if it is an electron, 0.3 Å if it is a H atom, and 0.05 Å if it is a Si atom. Consequently in solid state materials, where typical interatomic spacings are 1—3 Å, the wave nature of the electron will dominate over the particle behaviour. The electron interacts with many atoms at the same time and can easily tunnel in and out of many energy wells in the system. The motion of a 1 eV electron in a lattice, therefore, can only be described by including the quantum effects in the dynamics. On the other hand, the deBroglie wavelength of a 1 eV Si atom is so small that it can be correctly considered as a 'point' particle. The Si atom moves mainly in the classically allowed region of the configuration space. Therefore its motion is often well described by classical mechanics. The H atom is somewhere in between the two, and quantum corrections are often superimposed on the classical description of the motion. Potential surfaces or solutions to the electronic Schrödinger equation within the Born–Oppenheimer approximation, on the other hand, are only well known for a few systems. Recently, though, there has been a significant increase in the number and quality of interaction potentials for systems of interest to surface scientists.

The examples of molecular dynamics calculations of surface reactions that we could give in this article are ever increasing.[2] We have chosen to present work from our own group, and as a matter of convenience, have chosen examples that involve only one crystallographic arrangement of atoms – Si{001} and GaAs{001} surfaces. The first chemical reaction to be discussed is keV particle bombardment. With this approach, the kinetic energy of the primary particle exceeds the binding interactions normally present in chemical bonds. Because of this energy difference, a variety of novel and intriguing chain of events is rapidly set into motion subsequent to the impact event. Atoms may be significantly displaced from their equilibrium positions with old bonds broken and new ones formed. These phenomena have led to important applications. A major impetus for this research has been, of course, in the microelectronics area, where ion implantation of dopant ions and reactive ion etching of semiconductors are hot topics. There is also interest in evaluating surface processes which occur when energetic ions and molecules present in the space environment impinge on a diverse array of synthetic materials ranging from light metallic composites to protective polymer overlayers deposited on non-linear optical materials. The morphology of extraterrestial surfaces is believed to be influenced to some degree by interaction with the solar wind or other energetic ions. Of interest here is the use of the angular distributions of Ga^+ ions ejected from molecular beam epitaxially (MBE) grown crystals as a measure of the surface structure. This leads naturally into a discussion of how the microscopic reaction mechanisms of MBE growth proceed.

In MBE, atoms or molecules effuse from an oven source of material and impinge on a constant temperature substrate.[3] Depending upon growth conditions the film can have the same well defined crystalline structure as the underlying substrate (epitaxial) or it can have a random bonding structure (amorphous). The usual goal is to obtain layer-by-layer crystalline growth, for example, alternating bands of two layers of Si and two layers of Ge. Depending on the number of layers of each material the electronic properties such as the band-gap can be tailored to a desired value for a specific purpose. It is this control over the electronic properties that intrigues people in the electronics industry. To achieve this control, the layer growth must be almost perfect and thus it is of great interest to understand the fundamental reaction mechanisms so that we can propose new ideas for making higher quality films.

The construction of electronic devices not only involves growth processes such as MBE, but also involves etching of the material. One method of doing this is by keV particle bombardment, but one can also etch Si by reaction with F atoms. It is easy to imagine that the F atoms would react with unsaturated Si atoms on the surface because the Si–F bond strengths are quite strong at 5.0—7.0 eV. (Si–Si bonds are 2—3 eV.) After this step, it is unclear as to how and which silicon bonds will be broken in order to produce the gas-phase products,[4] predominantly SiF_4. Experimentally, it is found that during the initial exposure, the F atoms adsorb to the surface atoms forming the reaction intermediates $-SiF_x (x = 1,3)$.[5] As the F exposure is increased, the

---

Barbara J. Garrison received her B.S. Degree in Physics from Arizona State University in 1971 and her Ph.D. in Chemistry from the University of California, Berkeley in 1975. After a postdoctoral position at Purdue University and a Lectureship at UC Berkeley, she joined the Chemistry faculty at Penn State University in 1979 as an Assistant Professor. She is now Professor of Chemistry and Head of the Department. Her research interests include computer simulations of chemical reactions at surfaces such as keV particle bombardment, molecular beam epitaxy, diamond film growth, Si–F etching; many-body interaction potential development; and bonding at surfaces.

intermediates form a fluorosilyl adlayer 10—20 Å thick. The $-SiF$ and $-SiF_2$ species are thought to be located deeper in the adlayer near the silicon substrate with the $-SiF_3$ species terminating the surface.[5] The absolute amounts of the intermediates are still unresolved and the atomic structure of the adlayer has not yet been determined. Some very interesting chemical reaction questions are involved with this important processing procedure.

Our focus in the following sections will be on explaining the MD technique, exemplary interaction potentials, and the microscopic mechanisms of surface reactions of keV particle bombardment, MBE growth of Si, and F atom etching of Si.

2 Description of Molecular Dynamics Calculations

The details of performing molecular dynamics simulations can be subdivided into two basic parts. The first is the numerical solution of the classical equations of motion. Techniques for doing this are well developed so we will only briefly mention them here.[6] The other aspect of interest is the interaction potential for describing the forces among all the atoms. The development of these many-body interaction potentials is a current forefront research area. We will discuss two potentials that illustrate the different ways in which the problem can be approached.

2.1 Equations of Motion

Over 300 years ago Newton formulated the basic laws of classical mechanics. Of interest here to surface chemical reactions is the second law,

$$m_i\boldsymbol{a}_i = \boldsymbol{F}_i \tag{1a}$$

or

$$m_i d\boldsymbol{v}_i/dt = \boldsymbol{F}_i \tag{1b}$$

Figure 1 Sample keV particle bombardment event of a GaAs{001} surface. The Ga and As atoms are represented by blue/purple and yellow/green spheres, respectively. The incident Ar^+ ion is grey. Four frames are shown at 0, 50, 200, and 300 fs where 1 fs = 1×10^{-15} seconds. Initially the Ar^+ ion is moving towards the surface with 3 keV of kinetic energy.

or

$$m_i d^2\boldsymbol{r}_i/dt^2 = \boldsymbol{F}_i \tag{1c}$$

with

$$\boldsymbol{F}_i = -\nabla_i V(\boldsymbol{r}_1,\boldsymbol{r}_2,\ldots\boldsymbol{r}_n) \tag{1d}$$

where for n atoms, m_i, $\boldsymbol{r}_i$, $\boldsymbol{v}_i$, $\boldsymbol{a}_i$, and $\boldsymbol{F}_i$ are the mass, position, velocity, acceleration, and force of the i^{th} particle. The force can be obtained from the interaction potential $V(\boldsymbol{r}_1,\boldsymbol{r}_2,\ldots\boldsymbol{r}_n)$ for all the particles.

To obtain the positions and velocities as a function of time from equation 1, it is necessary to integrate the differential equations. The algorithms for doing this for the most part assume that the forces are constant over some timestep Δt. The solution is then propagated through time by using this approximation. To start the integration, initial conditions, in this case the positions and velocities, must be specified. In the example shown in Figure 1, we start all the atoms in the solid at assumed lattice positions and give them zero initial velocities. The kinetic energy and angle of approach of the incoming particle are known from the experimental conditions, thus we know the particle's initial velocity vector. The initial position of the incoming particle is a bit trickier to define. The coordinate above the surface must be large (usually 5—10 Å) so that it mimics a real experimental source a long distance from the surface. Unfortunately, the experimentalists cannot aim the primary particle 'head-on' towards a surface atom or directly between two surface atoms. Experimentally then, any datum is an average over many different aiming points on the surface. Consequently, in order to compare with experiment results, it is necessary to rerun the calculations many times with different aiming points on the surface.

Once the initial conditions and the interaction potential are known the classical equations of motion can be directly integrated. The 'results' of this integration are the positions and velocities of all the atoms as a function of time. The position data really represent a movie of all the atomic motions, snapshots of which are shown in Figure 1. All reaction mechanisms or atomic motions can be followed in exquisite detail. Moreover, the final positions of the atoms tell us, in particular, which ones have escaped into the vacuum and can subsequently be detected and which ones have rearranged in the solid. In the example shown in Figure 1, four particles eject, one from the first layer (yellow) and

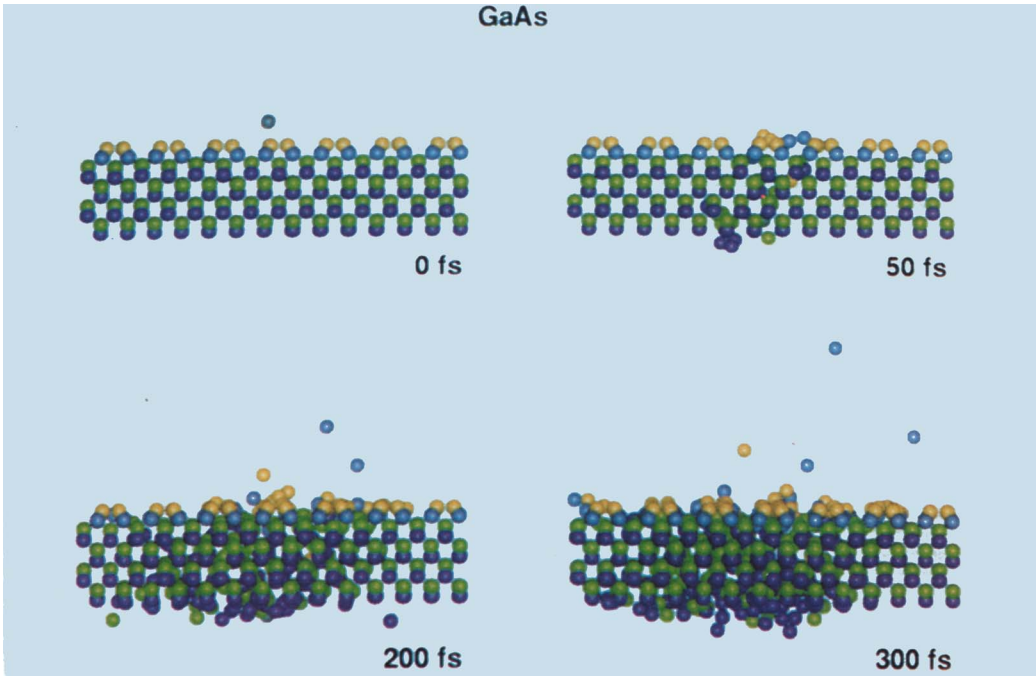

three from the second layer (blue). From the velocity vectors the energy ($E = \frac{1}{2}m\mathbf{v}\cdot\mathbf{v} = \frac{1}{2}mv^2$) and direction of motion of each particle can be computed. Energy and angular distributions are often measurable in experiments.[1] Of note is that both macroscopic quantities such as energy and angular distributions and microscopic quantities such as reaction mechanisms viewed as movies can be extracted from the classical picture. The real strength of the molecular dynamics simulations comes, however, when a correlation is found between the microscopic mechanisms and the quantities observed in experiments as will be discussed in Section 3.

There are three additional aspects of molecular dynamics simulations that should be mentioned before discussing the interaction potentials. These are time-step limitations, temperature control, and 'how to mimic an infinite solid?' The first two are features of all molecular dynamics simulations and the third is peculiar to the systems discussed here. As mentioned above, the critical assumption in numerical integrations is that the forces are constant over some Δt. The constancy of the force is determined by the interaction potential of choice. For those that apply to reactions, the acceptable timestep is about 1×10^{-15} seconds or 1 femtosecond (fs). Due to the speed of computers and ultimate round-off error problems, it is only feasible to calculate 10^6 to 10^8 timesteps, thus we are limited to simulating processes that occur shorter than 1—100 nanoseconds. This limitation is of no hindrance for keV particle bombardment (Section 3.1) but it is a problem for molecular beam epitaxy studies (Section 3.2).

Mimicking an infinite solid and temperature control can be approached in many ways. Only the methods used for the examples given here are discussed. For keV particle bombardment a slab of arbitrary size is chosen for a few test trajectories. Particles that want to leave through the sides or bottom are allowed to do so. In the real system they would go deeper into the solid taking their energy with them. Next, we test to see if this size is sufficiently large by making the slab bigger, rerunning the same trajectories and comparing the results. We finally choose a crystal size such that the quantities of interest are converged. In the case of the keV particle bombardment, the quantities of interest are the amount and identity of the particles that eject and their energy and angular distributions. Substrate damage has not been of interest to us so it is only necessary to choose a crystal size that is sufficiently large to mimic ejection but not damage. Temperature is not a significant perturbation to this system since the ejection process is over 100—500 fs whereas vibrational periods are ~ 1000 fs or ~ 1 ps.

A popular scheme to mimic an infinite solid is to use periodic boundary conditions with a slab of atoms as shown in Figure 2. Any particle that 'leaves' the left of the crystal then 'enters' on the right. The top surface towards the gas phase is of course free and generally the bottom surface is held rigid to keep this surface from reconstructing or rearranging. Periodic boundary conditions are more appropriate for processes that occur on longer timescales since small thermal motions must be taken into account. To maintain temperature control there are several layers in the slab. The top few layers are subject only to the forces from the interaction potential. The next few layers experience these same forces in addition to a force that maintains the system temperature. For example, one might include a friction term ($-\beta v$) where the friction coefficient, β, can be positive or negative depending on whether the system is too hot or too cold relative to the desired temperature.[7] This temperature control is critical for the exothermic deposition of atoms on the surface. For a real system of 10^{23} atoms, the excess energy will be dissipated. However, if there are only a few (several hundred) atoms, then the system will overheat or melt if some form of temperature control is not included.

2.2 Interaction Potentials

The validity of the simulation rests ultimately on the ability of the interaction potential to represent accurately the true chemical interactions. For many years two-body potentials were used for simulations. The assumption in two-body potentials is that the interaction between two atoms is independent of the presence of a third atom. A two-body description for H_3 would predict that it is three times more stable than H_2 whereas in reality H_3 is unstable. It is the development of *many-body* potentials for systems with hundreds of particles that makes these molecular dynamics simulations possible. For comparison purposes the two-body Lennard-Jones and Morse potential functional forms are given. In each case the total energy is written as

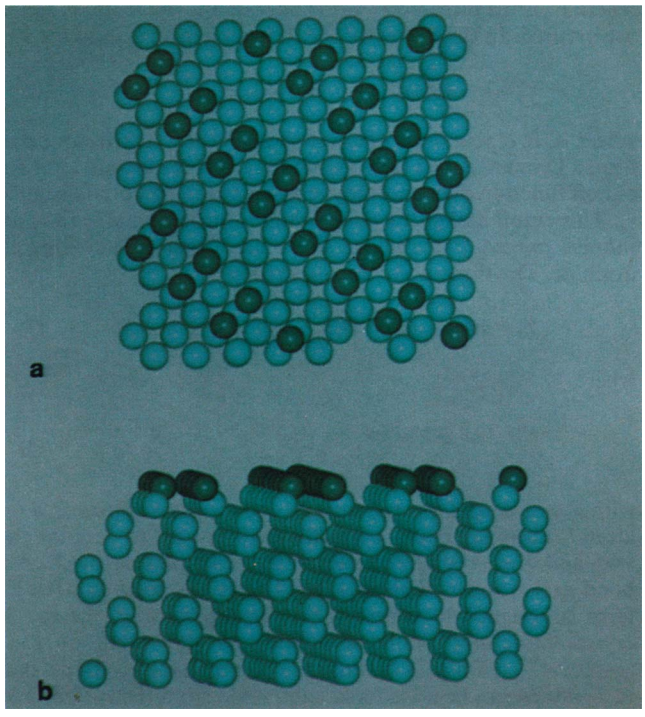

Figure 2 Top and side views of the (2 × 1) dimer reconstructed Si{001} surface. The Si atoms that are fourfold coordinated are depicted as light spheres. The surface atoms are represented by the dark spheres.

$$V(\mathbf{r}_1,\mathbf{r}_2\ldots\mathbf{r}_n) = \sum_i\sum_{j>i} V_2(r_{ij}) \tag{2}$$

where r_{ij} is the scalar distance between atoms i and j and V_2 is the two-body term. For a Lennard-Jones potential

$$V_2 = 4\epsilon[(\sigma/r_{ij})^{12} - (\sigma/r_{ij})^6] \tag{3}$$

where ϵ and σ are adjustable parameters. For a Morse potential

$$V_2 = D_e\{\exp[-2\alpha(r - r_e)] - 2\exp[-\alpha(r - r_e)]\} \tag{4}$$

where D_e, α, and r_e are the adjustable parameters. In both of these cases the atoms are represented by spheres and like a box of marbles, these Lennard-Jones or Morse atoms will pack in the closest array possible – a structure similar to copper metal or solid argon. Silicon and gallium arsenide, on the other hand, crystallize in a diamond lattice with each atom having four neighbours in a tetrahedral arrangement. It is mandatory then that many-body potentials be used for a realistic description of such systems. As two examples of many-body potentials we will discuss the Stillinger–Weber (SW) potential for Si/F and the Tersoff potential for Si.

The SW potential[8] is based on the complete expansion of the total interaction potential in 2,3,4... body terms as

$$V(\mathbf{r}_1,\mathbf{r}_2,\ldots\mathbf{r}_n) = \sum_i\sum_{j>i} V_2(r_{ij}) + \sum_i\sum_{j>i}\sum_{k>j} V_3(r_{ij},r_{ik},r_{jk}) + \ldots \tag{5}$$

where V_3 is the three-body term and four and higher body terms are omitted. In the SW work the following form is used for V_2,

$$V_2(r_{ij}) = A(Br_{ij}^{-p} - r_{ij}^{-q})\exp(c/r_{ij} - r_c) \quad (6)$$

where A, B, c, p, and q are parameters. The first term in equation 6 has a Lennard-Jones form (equation 3) and the second term is a cut off function that smoothly terminates the potential distance r_c. This cutoff makes the computations more tractable than an infinite ranged potential as there are fewer interactions to evaluate. The three-body term is written as

$$V_3 = H(r_{ij},r_{ik},\theta_{jik}) + H(r_{ji},r_{jk},\theta_{ijk}) + H(r_{ki},r_{kj},\theta_{ikj}) \quad (7)$$

where

$$H(r_{ij},r_{ik},\theta_{jik}) = \lambda\exp[\gamma/(r_{ij} - r_c) + \gamma/(r_{ik} - r_c)] \{\alpha(\cos(\theta_{jik}) - \beta)^2 - \rho\} \quad (8)$$

with λ, γ, α, β, and ρ as parameters and θ_{jik} the angle centred on atom i. There are many words that can be used to describe the two- and three-body interactions but the simplest is that V_2 is a bond stretch and V_3 is an angle bend in the SW potential. The V_3 term is designed to maintain the tetrahedral angle of the Si crystal structure (diamond lattice) as the value of β is cos(109.47°). Of note is that this is a potential for reactions, that is, Si atoms can be added and subtracted from the surface and the potential and forces are continuous and smooth.

For determining the Si–F interactions, Stillinger and Weber fitted the parameters in V_2 and V_3 to experimental data such as the lattice constant, the heat of sublimination, the elastic constants, and the melting temperature of Si; the energetics and geometries of SiF_x molecules; and whatever else they could find. The major portion of the creative work is to obtain reasonable functional forms. Fitting the parameters can be, however, a computational challenge.

In determining his potential for group IV elements (Si, Ge, and C), Tersoff[9] attacked the problem quite differently. His potential does not build on the expansion in many-body terms but is in actuality explicitly a three-body potential with implicit many-body interactions. He writes the interaction potential as

$$V(\mathbf{r}_1,\mathbf{r}_2,\ldots\mathbf{r}_n) = \tfrac{1}{2}\sum_i\sum_j[V_R(r_{ij}) + b_{ij}V_A(r_{ij})] \quad (9)$$

where V_R and V_A are the repulsive and attractive portions of the 'pair-like' interaction. The difference between this potential and a Morse potential (equation 4) is that the coefficient of the attractive term, b_{ij}, depends on the neighbours of atom i. Tersoff assumes

$$b_{ij} = (1 + \beta^n\zeta_{ij}^n)^{-\frac{1}{2}n} \quad (10)$$

with

$$\zeta_{ij} = \sum_{k\neq i,j}g(\theta_{jik})\exp[\lambda_3^3(r_{ij} - r_{ik})^3] \quad (11)$$

and

$$g(\theta_{jik}) = 1 + c^2/d^2 - c^2/[d^2 + (h - \cos\theta_{jik})^2] \quad (12)$$

In these equations β, ζ, λ_3, c, d, and h are parameters. The angular dependence is in the b_{ij} term but not in a straightforward manner. The difference between the Tersoff and SW angular dependences is that the Tersoff dependence does not pay a penalty for going away from a tetrahedral angle. This potential is still a functional form with parameters that must be fitted to experimental data. The Tersoff functional form allows one to fit Si_2 energetics as well as bulk Si properties which is not possible with the SW potential. Note that there are cutoff functions in the Tersoff potential which allow for speedier computations but these are not explicitly shown in equations 9 and 11 in order more clearly to illuminate the functional forms.

The ultimate test of any potential function is how well it predicts experimental data to which it was *not* fitted. Tests of these and other interaction potentials are continually in progress. The challenge ultimately will be to find more flexible functional forms, more experimental data to use in fitting the parameters, or perhaps a totally different manner in which to determine the interatomic forces on a computational timescale such that the forces can be evaluated during the simulation.[10]

3 Dynamics of Surface Reactions

The goal of using the molecular dynamics calculations is to better understand physical and chemical processes that occur in nature. Our contact to the real world is experimental data. Because of the space limitations we will concentrate here on the microscopic pictures that result from the MD calculations and will briefly mention the comparisons to experimental data. This priority is chosen to emphasize the aesthetic value of being able to visualize the microscopic world. Three MD simulations will be discussed. The first is the use of keV particle bombardment to determine structures of GaAs surfaces. The second is the molecular beam epitaxial growth of Si and the third is the F atom etching of Si surfaces.

3.1 Surface Structure Determinations of GaAs{001}(2 × 4)

The bombardment of solids by particles with keV of kinetic energy provides a dramatic example of how molecular dynamics simulations can be used to understand the basic reaction process as well as aid in the determination of surface structures. To put this energy regime in perspective, remember that bond strengths are usually in the order of 3—5 eV. The energetic particle, thus, has much more energy than the attractive interaction that binds atoms in the solid. Given this imbalance in energies, at first glance it is suprising that this process yields any useful information about the surface structure. However, we feel that the combination of MD simulations along with the experimental angular distributions of the ejected particles has been one of the major accomplishments in the use of MD for modelling surface reactions.[1]

The system of interest is GaAs{001}. There are over 30 structures of this surface depending upon the relative coverage of Ga and As.[11] The GaAs {001} surface is the template which is most widely used in the construction of microelectronic devices and has considerable technological relevance. Thus it is important to be able to characterize these structures in order to gain an atomistic picture of thin film growth. The approach that the group of Winograd at Penn State has used to examine these structures is to grow the GaAs{001} surfaces in a molecular beam epitaxy (MBE) chamber.[12] They then measure the angular distributions of the particles that are ejected as the result of keV particle bombardment. With MBE they force the top layer to be As atoms and thus the second layer contains Ga atoms.

The hypothetical or bulk-terminated unreconstructed GaAs{001} arsenic-terminated surfaces consists of a square array of As atoms (yellow) bonded to two Ga atoms (blue) in the layer below, as shown schematically in Figure 3. (Both Si and GaAs have structures in which each atom is tetrahedrally bonded to four other atoms.) Each As (or Si) atom possesses two partially filled 'orbitals' pointing upwards. Thus the As (or Si) atoms react to form dimers along this direction, doubling the lattice periodicity, as shown in Figures 2 and 3. In the laboratory, the (2 × 1) dimer reconstruction is observed for Si but not GaAs. A number of other reconstructions appear for GaAs, but we will concentrate on the (2 × 4). This structure has been suggested[13] by other techniques to be a dimerized surface with every 4th As-surface dimer missing, as shown on the right in Figure 3.

Since the focus of this paper is on the MD simulations, we will describe this project from the theoretical rather than the experimental perspective. In order to determine the effect of surface structure on the keV particle bombardment process, MD simu-

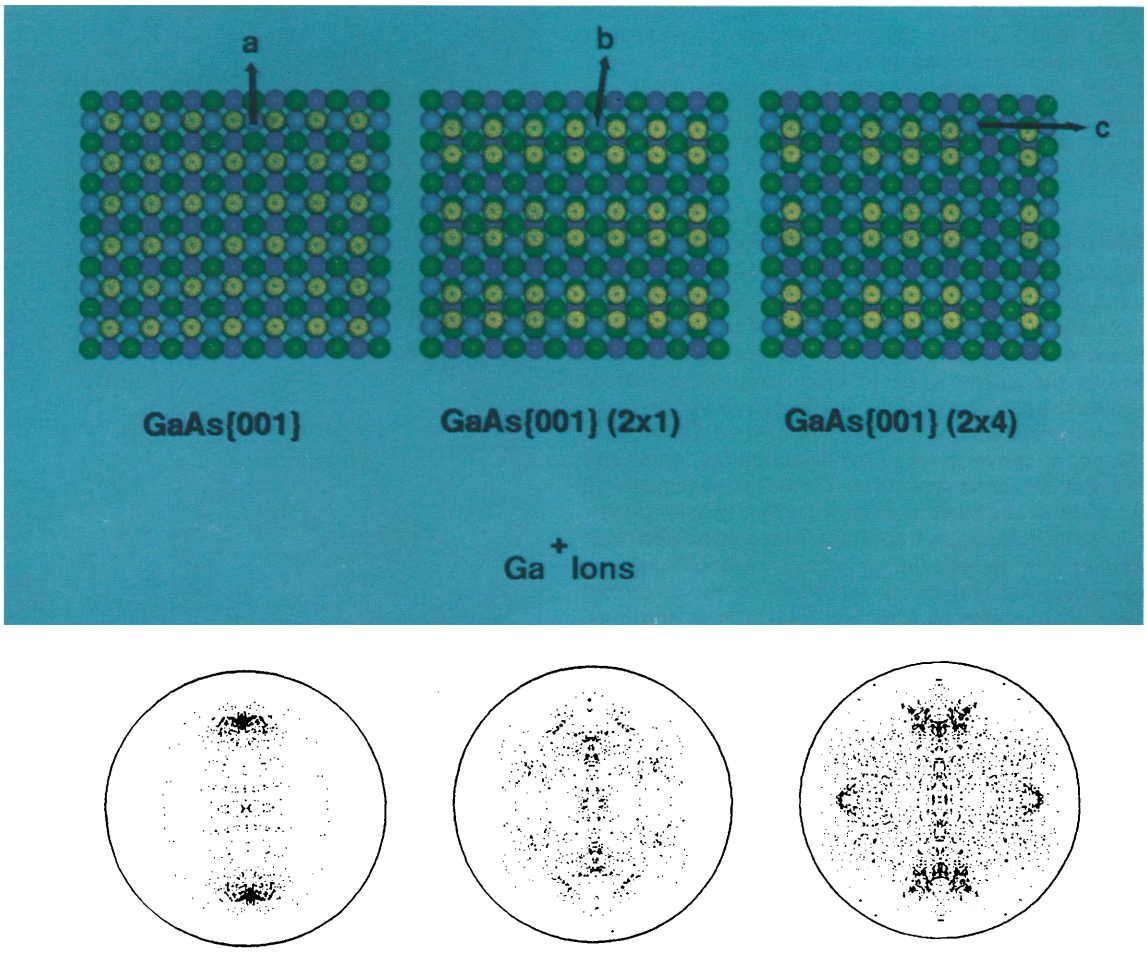

Figure 3 Top panel: Representations of three hypothetical GaAs{001} surfaces. The yellow spheres represent 1st layer As atoms; the blue spheres represent 2nd layer Ga atoms; the green spheres represent 3rd and 5th layer As atoms; and the purple spheres represent 4th layer Ga atoms. Bottom panel: Calculated angular distribution of 10—30 eV second layer atoms (Ga^+ ions in the experiment) desorbed by 3 keV Ar^+ bombardment of the corresponding surface shown in the top panel. The polar angle of emission is proportional to the distance of a spot from the centre of the circle. Ion ejection mechanisms (a), (b), and (c) are discussed in the text.

lations were performed for the three surfaces of GaAs as shown in Figure 3. One of the advantages of the MD simulations is that surface structures that cannot be fabricated in the laboratory can be constructed in the simulation. The incident Ar^+ ion beam had 3 keV of kinetic energy aimed perpendicular to a crystal with 2184 atoms. For each surface we ran 1000—3000 different aiming points in order to obtain statistically significant results. After running the MD simulations, the angular distributions of the particles that were ejected were computed from the known velocities. Of note is that the experimentalists measure only the Ga^+ ion distributions and that they know that the Ga is in the 2nd layer, thus only the angular distributions of atoms that originated from the 2nd layer are examined.[14] The angular distributions of the 2nd layer atoms are shown as spot patterns in Figure 3. The polar angle of emission is proportional to the distance of a spot from the centre of the circle. The orientation is the same as the surface shown above it.

The major features of the angular distributions of the Ga^+ ions (or second layer atoms) appear stepwise with the complexity of the reconstruction. For the bulk terminated surface there are two symmetrically equivalent directions of high intensity (spots) in the angular distribution. These appear almost identically along the direction between the 3rd layer As atom (green) and the 2nd layer Ga atom (blue) as is shown by the arrow labelled (a). As determined from the MD simulations, the dominant mechanism of ejection is a 3rd layer atom hitting a 2nd layer atom from behind and ejecting it. Note that there is plenty of room for the 2nd layer to escape from the surface. When the surface is dimerized (middle of Figure 3) many of the atom positions are shifted. There is now a trough between the dimer rows and the Ga atom direction is not as well collimated upon exit. Sidewings develop on the spots in the direction labelled by the (b) arrow. These sidewings become even more intense when there is a missing As surface dimer row (right side of Figure 3). In this (2×4) reconstruction the Ga^+ ions can now escape in the direction labelled by the (c) arrow at 90° relative to the major spots. The experimental measurements of these angular distributions agree quite nicely with the calculated distributions and show conclusively that the spot along the (c) direction is a signature of a missing surface As dimer.[14] The goal now is to start examining some of the other 29 proposed structures and also surface structures with small amounts of Al on the surface (precursors to Schottky barriers).

There is one issue that has not been mentioned. The experiments were performed on a GaAs crystal. The calculations were performed using Tersoff's interaction potential for Si. Why can we compare (successfully!) these two seemingly different sets of data? It is our belief, based on years of experience, that many of the processes and consequently the experimental results in the keV particle bombardment process are dominated by the relative positions of the atoms. This highly energetic process is not so sensitive to the precise chemical interactions. Silicon and GaAs have virtually identical structures and thus very similar angular

distributions to keV particle bombardment. The same conclusions hold true for metals. The angular distributions for all face-centred-cubic metals display the same predominant features. Details such as peak positions, intensities and widths do vary, however, with the chemical nature of the system. Chemical effects show up much more dramatically in processes such as MBE growth of Si and F atom etching of Si which will be discussed next.

3.2 Molecular Beam Epitaxial Growth of Si{001}(2 × 1)

Molecular-beam epitaxy (MBE) is widely employed for semiconductor epitaxial film growth.[3] The quality of the electronic device is related to the perfection of the layers of material. One of the problems with obtaining layer-by-layer growth is the fact that atoms in the surface layer of most semiconductors are significantly displaced from the bulk configuration. As discussed above, the surface atoms on the bulk terminated Si{001} face (Figure 2) tend to move closer to the neighbouring atoms and form rows of stable dimer structures. These rearrangements do not only constitute the basis of esoteric surface physics experiments, but are also extremely important from a microelectronic device point of view. In order for epitaxial growth to occur on a reconstructed surface (Figure 2), the atoms in the dimerized surface layer must reorder back to their original bulk positions, so that the atoms in the deposited layer are in the expected bulk positions for the next higher layer. It is the question of the dimer opening that we wish to assess with the MD technique.

The molecular dynamics simulation[15] consisted of 10 layers of silicon with 32 atoms per layer as shown in Figure 2. As mentioned above, the atoms in the bottom layer were anchored in position with the atoms in the next four layers forming a stochastic region. The atoms in the top five layers and all the deposited atoms were considered 'real atoms' and moved only under the influence of the interaction potential. The deposition rate of thermal energy Si atoms, at 1 atom per 2—3 ps (1 ps = 10^{-12} second), was sufficiently slow as to allow equilibration of the system before the arrival of the next atom. It has been pointed out in an earlier study[16] that if the deposition rate is too fast to allow for complete dissipation of the kinetic energy from exothermic adsorption reactions, the excess energy in the interaction region effectively destroys the structure of the interface between the originally reconstructed surface and the layers of the deposited material. The effect of long-time equilibration after the deposition, in that case, is like the simulation of crystallization from a liquid state. After each deposition of 1.5 monolayers of atoms the full system was equilibrated for 0.5 to 1 ns. The dynamic behaviour of the deposited and the substrate atoms revealed microscopic and macroscopic features of the growing film.

The predominant adsorption process is the attachment of the incoming Si atom to one of the radical orbitals on the surface dimer Si atoms. In the left frame of Figure 4a, Si adatoms are shown on the radical orbital of each of the surface dimer atoms. (The third Si adatom is attached to an adjacent Si dimer atom and is not in the gas phase.)

The microscopic mechanisms of dimer openings can be broadly categorized into two types.[15] First is the diffusing adatom induced mechanism, typical examples of which are shown in Figures 4(a,b). The Si adatom moves as shown by the arrows in Figure 4a during the equilibration period (0.5—1.0 ns). Initially both the radical orbitals of an isolated dimer are saturated with two adatoms. A third adatom diffuses over a period of hundreds of picoseconds, to move closer to the dimer, and pushes the adatom on the radical orbital into the epitaxial position. The diffusing adatom itself then occupies the vacant radical orbital of the open dimer. The three adatoms finally occupy the epitaxial positions, whereas the surface dimer atoms have relaxed back to their bulk positions. Another observed mechanism of the diffusing adatom induced dimer opening is shown in Figure 4b. Instead of pushing the adatom on the radical orbital into the epitaxial position, in this case, the

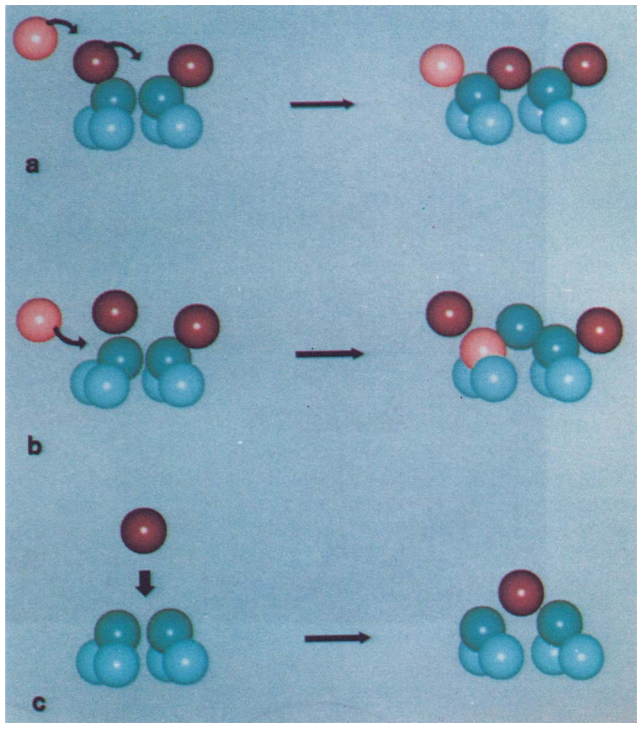

Figure 4 Diffusing adatom motion induced mechanisms of dimer openings. Only a subset of the atoms are shown. The same colour scheme as in Figure 2 is used. The deposited Si adatoms are shown as various shades of peach spheres. (a) Epitaxial growth. (b) Defect formation. (c) Direct dimer opening from adatom deposition.

diffusing adatom can move underneath the adatom on the radical orbital and push the dimer atom into the epitaxial position. Here the diffusing adatom has moved into the top substrate layer whereas the substrate dimer atom has moved up into the epitaxial layer. The end products, as shown in Figures 4a and 4b, in the homoepitaxy of Si or Ge are identical. However, in case of the heteroepitaxy of Ge on Si this second mechanism will cause the formation of a defect at the interface. This defect is formed during the growth event and is not due to interlayer diffusion during an annealing process. In other words, the final configuration in Figure 4a does not convert into the one in Figure 4b and *vice versa* during annealing.

The atoms in a surface dimer are constantly vibrating about their equilibrium positions with amplitudes determined by the temperature of the substrate. The second mechanism of dimer opening occurs when an incoming adatom is directly inserted into the available epitaxial position, thus stabilizing the opening. We found that the direct insertion of the adatom into epitaxial positions can occur on a bare dimer (Figure 4c), on a dimer with one radical orbital occupied, and also on a dimer with both of its radical orbitals occupied. Most of such direct insertion mechanisms occurred during the deposition process, *i.e.* the surface was relatively clean. The number of such occurrences increased with an increase in the temperature of the substrate.

The computations described in this section are quite extensive by today's standards as they took the equivalent of over a month of dedicated time on an IBM 3090 computer. There were several hundred atoms in the system and a total time of 3.5×10^{-9} seconds was simulated for the growth of 4—5 layers of material. However, the experimental conditions are such that a layer is grown in 1 second to 1 minute! For the near future these times will be impossible to simulate with MD because in MD we must use timesteps on the order of 10^{-15} seconds. The main physical process that is missing in the simulation is diffusion of the

deposited atoms on the surface. In fact, the atoms do move many lattice positions before finally incorporating into the crystal. Other techniques such as transition state theory are now being applied to examine these long term effects.[17] These results of the transition state calculations compare favourably with the observed activation energies of diffusion and the direction anisotropy.[18]

3.3 F Atom Etching of Silicon

The atomic mechanisms responsible for the formation of the gas-phase products observed during the etching of silicon by fluorine atoms and the structure of the surface during the etching process are quantities of interest in the Si–F study. The Stillinger and Weber potential energy function which describes the interaction between Si and F atoms has been used.[5] For the purpose of simulating the initial stages of fluorine adsorption on the Si{100}(2 × 1) surface, a microcrystallite of ten layers of silicon atoms with 32 atoms per layer and horizontal periodic boundary conditions was used.[19] The surface atoms were arranged into the dimer reconstructed surface and a F atom was attached to each dangling bond. Estimates of the kinetic energy of F atoms in plasmas are between thermal and 8 eV,[20] thus in order to overcome the barriers for reaction, F atoms with 3 eV of kinetic energy were used. A total of 200 F atoms were eventually adsorbed onto the surface. At this point a steady-state condition is reached such that the rate of deposition of F atoms equals the rate of F atoms leaving the surface in products such as SiF_4. To our knowledge this is the first molecular dynamics calculation in which a near steady-state reaction condition of an observed macroscopic process has been simulated.

Figure 5 F atom etching of Si. The yellow spheres represent non-fluorinated Si atoms, the green, mauve, red, and light blue spheres represent mono-, di-, tri-, and tetrafluorinated Si atoms. The dark blue and black small spheres represent F atoms. (a,b) Top and side views of the surface at the end of the simulation. (c—f) Formation of a gaseous SiF_4 molecule from the reaction between the incoming fluorine atom (black sphere) with an SiF_3 adspecies.

The surface configurations during the simulation were examined in order to elucidate the possible structure of the experimentally observed fluorosilyl layer. In Figure 5(a,b) we display the surface configuration after the last fluorine adsorption event. At this time almost two of the original layers of silicon atoms are etched. Only the top five layers of the crystal are depicted. Upon examination of this surface, there are many scattered vacant regions which are created by the etching of silicon atoms. The vacancies are scattered inhomogeneously across the surface due to the random nature of the etching process. Moreover, the surface configuration has evolved such that it is difficult to locate the position of the dimer rows of the initial defect free surface. Some interlayer mixing has also occurred. More information regarding the typical surface structure is revealed when the surface configuration is examined for local structure. For instance, some pairs of adspecies dimerize while others retain approximately the bulk geometry of the silicon lattice. In addition to the bonding between pairs of adspecies, there are groups of three adspecies where the bonding direction is nearly perpendicular to the surface plane, forming a tower-like structure. These structures are attached to the solid through the SiF and SIF_2 moieties and can either still be in the solid or protrude into the vacuum. One tower with the composition SiF–SiF–SiF_3 (green–green–red spheres) appears in the middle of Figure 5b. For all the tower structures, the SiF and SiF_2 are adspecies which lengthen the tower whereas the SiF_3 are adspecies which terminate the tower at the vacuum–surface interface. This observation would suggest that a type of layering occurs while the surface is being fluorinated. The fraction of fluorine in the different layers at the end of the simulation suggests that the first layer silicon atoms are mainly SiF_2 adspecies, the second layer silicon atoms are mainly SiF adspecies while the third and fourth layers are just beginning to be fluorinated. Thus, a sequential fluorination appears to be occurring in the crystal, starting with the first layer and progressing deeper into the crystal. This observation of the SiF_x layering agrees with conclusions drawn from surface science experiments.[5]

The results from the MD calculations illustrate a mechanism responsible for the major gas-phase product, SiF_4, as is shown in Figure 5. The initial configuration is a SiF_3 adspecies with its

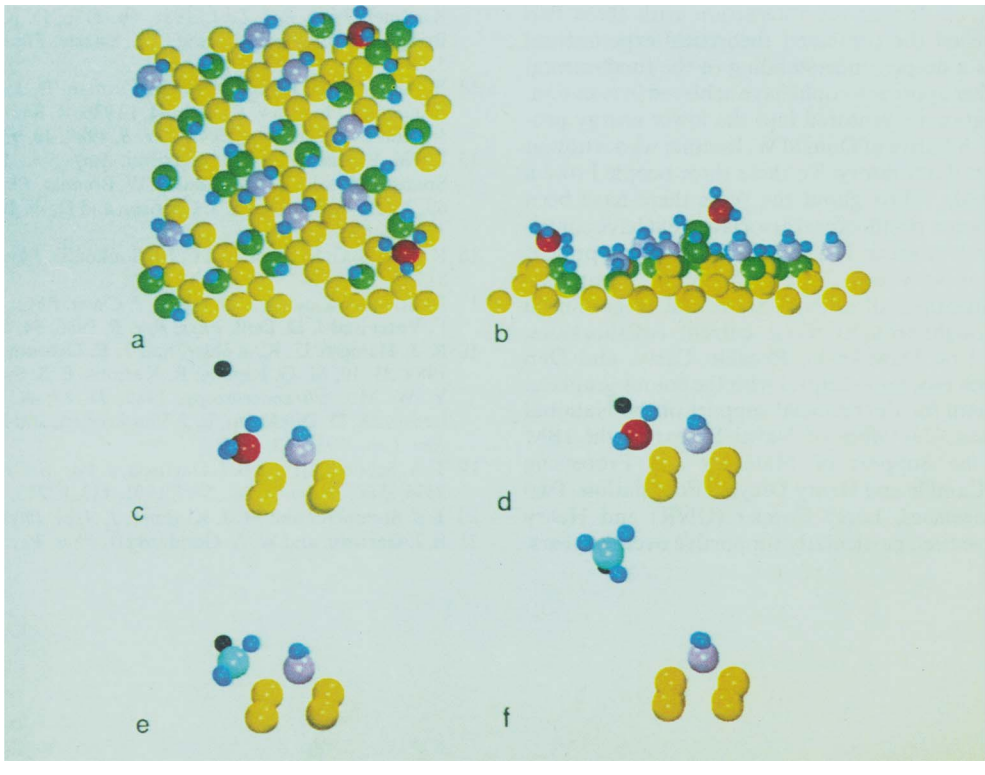

Si–F bonds directed into the vacuum. As the fluorine atom approaches the silicon atom, the Si–F bonds invert from extending into the vacuum (Figure 5c) to being planar with the silicon atom (Figure 5d) to being directed towards the surface (Figures 5e,f). During the reaction the Si–Si bond lengthens and breaks. This umbrella type motion of the Si–F bonds typifies the S_N2 reaction as suggested by *ab initio* electronic structure calculations.[21] As a final note, we have proposed that the tower-like features are the precursors to the etch products Si_2F_6 and Si_3F_8.

4 Conclusion

Molecular dynamics simulations have an attractive appeal in that they can supply pictures of *microscopic* reaction events that seem eminently plausible. The ultimate challenge is to determine their connection to nature. Consequently there should be continual interaction of the computer simulators with the experimentalists. Where possible, calculated results should be compared with experimental data. The experimentalists should look upon the results of the calculations as challenges to prove or disprove. Over the years we have found that this synergistic approach has led to the understanding of surface reactions to a greater depth than would have been achieved if either the theorists or experimentalists were working in isolation.

The use of molecular dynamics and other types of computer simulations will continue to grow. Computers are becoming even faster. The graphics for visualization of the results are becoming better and easier to use. The interaction potentials are becoming more sophisticated, and, as they are tested and improved, their reliability becomes even better.

Finally, we have chosen three examples from our own work to highlight in this article. We by no means wish to imply that others are not pursuing similar directions, either for surface reactions or reactions in other media such as liquids, biological compounds, and polymers.

Acknowledgements. The ventures into the detailed understanding of the keV particle bombardment process were initiated in 1977 in collaborations with Nicholas Winograd of Penn State University and the late Don E. Harrison, Jr. of the Naval Postgraduate School. It was the interaction with these two people that propelled the combined theoretical/experimental approach towards a deeper understanding of the fundamental processes than either approach could have achieved in isolation. Our research programme ventured into the lower energy processes through the initiative of Donald W. Brenner who is now at the Naval Research Laboratory. To these three people I owe a big debt of gratitude. Throughout the years there have been numerous students and postdoctoral associates that have contributed to the research projects. The people whose work is present here include Deepak Srivastava, Tracy Schoolcraft, Kevin Caffey, and Rik Blumenthal, all of Penn State, and Roger Smith (University of Loughborough). Four current collaborators, Ramona Taylor, Eric Dawnkaski, Recaldo Carty, and Dan Bernardo have been especially helpful with the colour graphics. Finally I am grateful for the financial support of the National Science Foundation, the Office of Naval Research, the IBM Programme for the Support of Materials and Processing Sciences, and the Camille and Henry Dreyfus Foundation. Two people at these agencies, Larry Cooper (ONR) and Henry Blount (NSF), have been particularly supportive over the years. Penn State University has supplied a generous grant of computer time for these studies.

5 References

1 N. Winograd and B. J. Garrison, in 'Ion Spectroscopies for Surface Analysis', ed. A. W. Czanderna and D. Hercules, Plenum Press, 1991, pp. 45—141 and references therein.
2 For example, U. Landman, W. D. Luedtke, N. A. Burnham, and R. J. Colton, *Science*, 1990, **248**, 454; R. A. Stansfield, K. Broomfield, and D. C. Clary, *Phys. Rev.*, 1989, **B39**, 7680; T. J. Raeker, D. E. Sanders, and A. E. DePristo, *J. Vac. Sci. Technol.*, 1990, **A8**, 3531; J. C. Tully, *J. Chem. Phys.*, 1980, **73**, 6333; M. S. Daw and M. I. Baskes, *Phys. Rev. Lett.*, 1983, **50**, 1285; D. W. Brenner, B. I. Dunlap, J. W. Mintmire, R. C. Mowrey, and C. T. White, 'Proceedings of the Second International Conference on New Diamond Science and Technology', ed. by R. Messier and J. T. Class, MRS International Conference Proceedings Series, Materials Research Society, Pittsburgh, PA, 1991, p. 39.
3 J. C. Bean, *Phys. Today*, 1986, **39**, 36.
4 F. A. Houle, *J. Appl. Phys.*, 1980, **60**, 3018; H. F. Winters and F. A. Houle, *J. Appl. Phys.*, 1983, **54**, 1218; F. A. Stevie and M. J. Vasile, *J. Appl. Phys.*, 1982, **53**, 3799; and H. F. Winters and I. C. Plumb, *J. Vac. Sci. Technol.*, 1991, **B9**, 197.
5 F. R. McFeely, J. F. Morar, N. D. Shinn, G. Landgren, and F. J. Himpsel, *Phys. Rev. B*, 1984, **30**, 764; F. R. McFeely, J. F. Morar, and F. J. Himpsel, *Surf. Sci.*, 1986, **165**, 277; C. W. Lo, D. K. Shuh, V. Chakarian, K. A. German, and Y. A. Yarmoff, submitted to *Phys. Rev. B.*
6 W. G. Hoover, 'Molecular Dynamics', Lecture Notes in Physics #258, Springer-Verlag, Berlin, 1986; D. W. Heermann, 'Computer Simulation Methods in Theoretical Physics', Springer-Verlag, Berlin, 1986.
7 H. J. C. Berendsen, J. P. M. Postma, W. F. van Gunsteren, A. Dinola, and J. R. Haak, *J. Chem. Phys.*, 1984, **81**, 3684.
8 F. Stillinger and T. Weber, *Phys. Rev.*, 1985, **B31**, 5262; F. H. Stillinger and T. A. Weber, *Phys. Rev. Lett.*, 1989, **62**, 2144; T. A. Weber and F. H. Stillinger, *J. Chem. Phys.*, 1990, **92**, 6239.
9 J. Tersoff, *Phys. Rev. Lett.*, 1988, **61**, 2879; J. Tersoff, *Phys. Rev.*, 1989, **B39**, 5566.
10 R. Car and M. Parrinello, *Phys. Rev. Lett.*, 1985, **56**, 2471.
11 J. H. Neave and B. A. Joyce, *J. Cryst. Growth*, 1978, **44**, 387.
12 R. Blumenthal, S. K. Donner, J. L. Herman, R. Trehan, K. P. Caffey, E. Furman, and N. Winograd, *J. Vac. Sci. Technol.*, 1988, **B6**, 1444; R. Blumenthal, Thesis, The Pennsylvania State University, 1990.
13 M. D. Pashley, K. W. Haverern, W. Friday, J. M. Woodall, and P. D. Kirchner, *Phys. Rev. Lett.*, 1988, **60**, 2176; D. K. Biegelsen, R. D. Bringans, J. E. Northrup, and L. E. Swartz, *Phys. Rev. B*, 1990, **41**, 5701.
14 R. Blumenthal, K. P. Caffey, E. Furman, B. J. Garrison, and N. Winograd, *Phys. Rev. B*, 1991, **44**, 12 830; R. Smith, D. E. Harrison, Jr., and B. J. Garrison, *Phys. Rev. B*, 1989, **40**, 93.
15 D. W. Brenner and B. J. Garrison, *Surf. Sci.*, 1988, **198**, 151; D. Srivastava, B. J. Garrison, and D. W. Brenner, *Phys. Rev Lett.*, 1989, **63**, 302; D. Srivastava, B. J. Garrison and D. W. Brenner, *Langmuir*, 1991, **7**, 683.
16 R. Biswas, G. S. Grest, and C. M. Soukoulis, *Phys. Rev. B*, 1988, **38**, 8154.
17 D. Srivastava and B. J. Garrison, *J. Chem. Phys.*, 1991, **95**, 6885; A. F. Voter and J. D. Doll, *Phys. Rev. B*, 1986, **34**, 6819.
18 R. J. Hamers, U. K. Köhler, and J. E. Demuth, *Ultramicroscopy*, 1989, **31**, 10; M. G. Lagally, R. Kariotis, B. S. Swartzentruber, and Y. W. Mo, *Ultramicroscopy*, 1989, **31**, 87; A. J. Hoeven, J. M. Lenssinck, D. Dijkkamp, E. J. Van Loenen, and J. Dieleman, *Phys. Rev. Lett.*, 1989, **63**, 1830.
19 T. A. Schoolcraft and B. J. Garrison, *J. Vac. Sci. Technol. A*, 1990, **8**, 3496; *ibid.*, *J. Am. Chem. Soc.*, 1991, **113**, 8221.
20 T. J. Sommerer and M. J. Kushner, *J. Appl. Phys.*, 1990, **70**, 1240.
21 B. J. Garrison and W. A. Goddard III, *Phys. Rev. B.* 1987, **36**, 9805.